Superconductive tendencies of strange metals

January 2023
Agisilaos Papatheodorou

B.S. Aristotle University of Thessaloniki

M.S. Utrecht University

Directed by professor H.T.C Stoof

Abstract

Motivated by recent ARPES experiments on strange metals, we implement those measurements to the standard condensed-matter theory. Considering that the best description is found to be a nodal self-energy similar to that of the Gubser-Rocha model, derived by AdS/CFT calculations, we are encouraged to match this term's analytical properties to the standard formalism and calculate the critical temperature corrections produced. Comparing it with the standard BCS prediction, we evaluate whether such correction has a tendency to higher temperature superconductivity.

Table of contents

List of Figures

List of Tables

Introduction

The unexpected discovery of high-temperature superconductors (HTS) stirred up the world of condensed-matter physics as Bednorz and Müller measured a critical temperature of $35K$ for the cuprate lanthanum-barium-copper oxide well above anything measured beforehand (1986). HTS find large-scale applications in the heart of modern physics like the Large Hadron Collider at CERN being driven by super-cooled bismuth-strontium-calcium-copper oxide superconductors. Despite their technological applications, these strange metals appeal to the scientific community mainly for eluding any of the standard microscopic theoretical treatments like the very successful Bardeen–Cooper–Schrieffer (BCS) theory. Consequently, alternative theoretical descriptions like the recent superexchange [1] interaction models and the Anti-de Sitter/Conformal field theory or AdS/CFT correspondence gain popularity for battling this theoretical deficiency. This script focuses on the later, as new evidence surfaced, provoking great scientific interest in finding out how its intricate nature can describe the reality of strange metals. Originating in 1997 by Juan Maldacena [2][3], this approach merges string theory on AdS spaces with a conformal field theory, using Gerard 't Hooft's holographic principle in order to find the conjecture of a strongly correlated condensed matter system with a weakly interacting gravitational one of one higher dimension.

The success of this theory lies in describing the intricate frequency [4] and recently found momentum dependence [5] of the nodal self-energy of strange metals. In the context of holography, this self-energy originates from a gravitationally dual model with the purpose of describing an electron interacting with a CFT near its superconducting phase transition region. This special behaviour is encaptured into the critical exponent, which in the case of strange metals, bridges the gap between Fermi liquid and non-Fermi liquid as shown by the best experimentally fitted spectral function [5]. From this fact follows that the critical exponent must be momentum dependent [3].

Following the instructions of condensed-matter theory we evaluate whether the analytical properties of the Gubser-Rocha self-energy, containing the critical exponent, matches the standard formalism by studying it on the complex plane. The analytic properties of the propagator are then derived which is followed by an assessment of the spectral function's ability to follow the quantum mechanical rulebook.

Having attained enough information we present the formalism which will lead to a critical temperature calculation for a many-body system of fermions and attempt to go through it with the additional self-energy corrections. The continuous nature of the

critical exponent stands as an obstacle in these kind of calculations so the resulting critical temperature is given for a simplified form of a momentum independent critical exponent at optimal doping and a approximate general form where the real part of the self-energy has been singled out. For the later, the Gubser-Rocha critical exponent range is matched with that of the experiment [5] and the calculations are conducted along a numerical approximation.

Evaluating the results and methods used in this script, we then present the superconductive contribution of the nodal self-energy to the critical temperature and asses its importance.

Strange metal self-energy in second-quantization formalism

1 Experimental self-energy and the Gubser-Rocha form

Fitting angle-resolved photoemission of $(Pb,Bi)_2Sr_{2-x}La_xCuO_{6+\delta}$ for different momenta and temperatures [5] the calculated spectral function follows a Lorentzian shape, which later becomes asymmetric away from the transition point hinting towards momentum dependent exponent terms. The width Γ_H of that spectral function is then identified with the imaginary self-energy $\Sigma''(k,\omega)$. The modified fit-function $L_H(k)$ is of the form:

$$\begin{aligned} L_H(k) &= \frac{W}{\pi}\frac{\frac{\Gamma_H}{2}}{(k-k_*)^2+(\frac{\Gamma_H}{2})^2}, \\ \Gamma_H(k) &= G_0+\lambda\frac{[(\hbar\omega)^2+(\beta k_B T)^2]^{\alpha(k)}}{\hbar\omega_N^{2\alpha(k)-1}}, \\ \alpha(k) &= a(1+V[\frac{k-k_F}{k_F}]). \end{aligned} \tag{1}$$

In these equations λ and β are fitting parameters normalized to an energy scale of ω_N, while G_0 is the self-energy contribution from impurity scattering, V the asymmetry parameter. It is worth noting that the doping dependence is included in the α coefficient which takes the value of $a = 0.51$ for optimal doping up to the value of $a = 0.84$ for the most overdoped state. The width Γ_H of the Lorentzian curve is

directly connected with the imaginary part of the self-energy[6], as

$$\Sigma''(k,\omega) = \frac{v_F \Gamma_H(\omega,k)}{2} \propto \omega^{2\alpha(k)}, \tag{2}$$

where $v_F$is the Fermi velocity.

Considering momentum-dependent exponents, the Gubser-Rocha model [4] provides an excellent candidate where the theoretically produced self-energy has frequency dependence with a momentum-dependent power-law. We denote this critical exponent by ν_k and identify it with $a(k)$. For zero temperatures this self-energy is defined by the equation

$$\Sigma(k,\omega) = g\omega(-\omega^2)^{\nu_k - \frac{1}{2}}. \tag{3}$$

Notably, the asymmetry parameter V is required to take the value of minus one for the Gubser-Rocha self-energy to match the experiment although fixing the rest of the parameters and fitting the ARPES data again yields a similar value for V [5].

We can see how these terms coalign by performing an $\varepsilon << 1$ expansion of the form $\omega \to \omega + i\varepsilon$ and neglecting ε^2 terms. This yields:

$$\Sigma(k,\omega) = g(\omega + i\varepsilon)e^{(\nu_k - \frac{1}{2})\ln(-\omega^2 - 2i\varepsilon\omega)} \tag{4}$$

Looking at the complex plane on Fig.(1) the orange region is found for $\omega < 0$ and the red one for $\omega > 0$. The arguement of the complex $z = -\omega^2 - 2i\omega\varepsilon$ can be found as

$$arg(z) = \begin{cases} +\pi & ,\omega < 0 \\ -\pi & ,\omega > 0\ . \end{cases}$$

It bares mention that the branch cut created by the logarithm of Eq.(4) spans across the whole real axis on the ω plane but is restricted for the complex z plane, as the positive region is inaccessible for any ω. Knowing this, the self-energy can be written as

$$\Sigma(\omega,k) = \pm g|\omega| e^{(\nu_k - \frac{1}{2})\ln|\omega|^2} e^{\mp(\nu_k - \frac{1}{2})i\pi} = \pm g|\omega||\omega|^{2\nu_k - 1}[cos(\mp(\nu_k - \frac{1}{2})\pi) + isin(\mp(\nu_k - \frac{1}{2})\pi)], \tag{5}$$

where the top sign corresponds to $\omega > 0$ and the bottom one to $\omega < 0$.

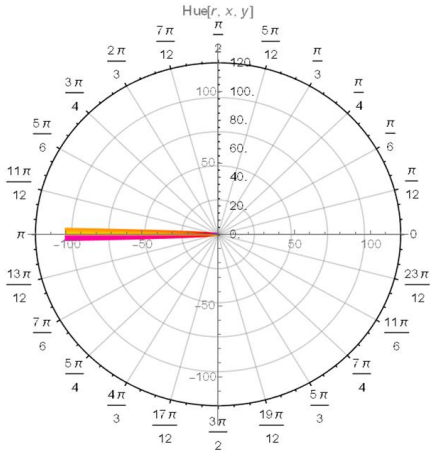

Figure 1: Contour graph of $\Sigma(\omega,k)$ in the polar ω^2 plane.

The real and imaginary part of the Gubser-Rocha self-energy now become

$$\begin{aligned} Re(\Sigma(k,\omega)) &= \pm g|\omega|^{2\nu_k} cos(\mp(\nu_k-\frac{1}{2})\pi) - \varepsilon g|\omega|^{2\nu_k-1} sin(\mp(\nu_k-\frac{1}{2})\pi) \\ Im(\Sigma(k,\omega)) &= \pm g|\omega|^{2\nu_k} sin(\mp(\nu_k-\frac{1}{2})\pi) + \varepsilon g|\omega|^{2\nu_k-1} cos(\mp(\nu_k-\frac{1}{2})\pi)\ . \end{aligned} \tag{6}$$

Taking the limit $\varepsilon \to 0^+$ yields:

$$\begin{aligned} Re(\Sigma(k,\omega)) &= g\omega|\omega|^{2\nu_k-1} cos((\nu_k-\frac{1}{2})\pi), \\ Im(\Sigma(k,\omega)) &= -g|\omega|^{2\nu_k} sin((\nu_k-\frac{1}{2})\pi). \end{aligned} \tag{7}$$

Identifying α with ν_k, the Gubser-Rocha imaginary self-energy shows exactly the same $\Sigma''(\omega,k) \propto \omega^{2\alpha(k)}$ relation as the experiment.

Constructing the propagator

2.1 Application to the condensed-matter formalism

The aim of this subsection is to gain insight about the Gusber-Rocha self-energy in the full complex plane. Consequently, we analytically continue the frequency $\omega = x + yi$ and split the self-energy into a real and an imaginary part once more.

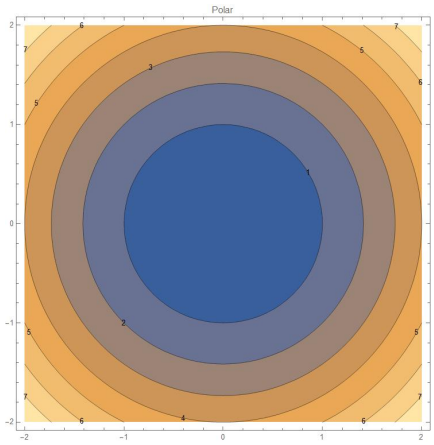

Figure 2: Absolute value of the $-\omega^2$ function in the complex plane.

Graphing and verifying the structure of such function can prove to be somewhat tedious since branch cuts take away its continuity and complex inputs to the logarithmic function create a multiplicity of solutions called Riemann sheets. Since most visualization softwares do not take well to those traits we will be breaking down this procedure focusing first on the behaviour of the multi-valued $-\omega^2$ function for complex frequencies as a sanity check. The starting shape of Fig.(2) must remain consistent when we combine it with the rest of the self-energy terms. Consequently, the next step entails raising the previous function to the rational power of $\nu_k - \frac{1}{2}$ and multiplying by the complex frequency. Calculating the complete self-energy using cartesian coordinates, with $\omega = x + yi$, yields

$$\begin{aligned}\Sigma(k,x,y) = g[x(x^2+y^2)^{\nu_k-\frac{1}{2}}cos((\nu_k-\frac{1}{2})\theta) - y(x^2+y^2)^{\nu_k-\frac{1}{2}}sin((\nu_k-\frac{1}{2})\theta)] \\ + ig[y(x^2+y^2)^{\nu_k-\frac{1}{2}}cos((\nu_k-\frac{1}{2})\theta) + x(x^2+y^2)^{\nu_k-\frac{1}{2}}sin((\nu_k-\frac{1}{2})\theta)],\end{aligned} \tag{8}$$

where θ is the angle of the complex number $-\omega^2$. Since this negative exponentiated term creates a branch cut on the real axis of the complex ω plane one should be careful as to not cross to another Riemann sheet.

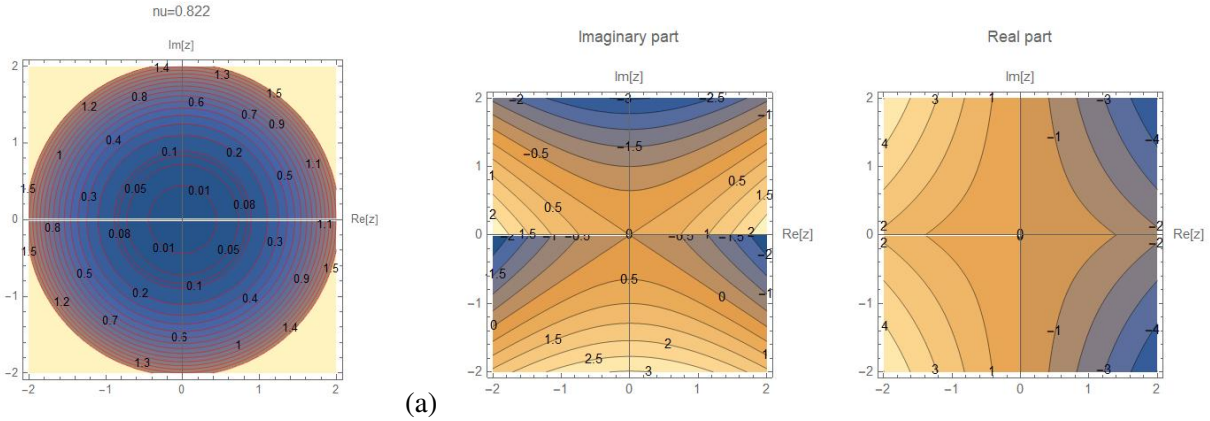

(a) (b)

Figure 3: (a) Example of the absolute value of the self-energy Σ, (b) example of the real and imaginary part of the self-energy in the complex ω plane for the critical exponent value of $\nu_k = 0.822$

It is worth noting that the imaginary self-energy of Fig.(3. b) takes both negative and positive values on the upper and lower complex plane. This is an unusual feature for condensed matter systems which will prove to be cumbersome, as shown later in the script.

To unravel the properties of an interacting system dictated by the Gubser-Rocha self-energy we turn our attention the Green's function derived in the Lehmann representation [7]. Close to the real axis the non-interacting Green's function is given by the typical form

$$G_0(k,\omega) = \frac{\hbar}{\hbar\omega - (\varepsilon_k - \mu)}. \tag{9}$$

In the interacting case an imaginary part is added to the denominator that comes from the self-energy, which is related to the lifetime of the excitation causing the interaction as

$$G(k,\omega) = \frac{\hbar}{\hbar\omega - (\varepsilon_k - \mu) - \hbar\Sigma(k,\omega)}. \tag{10}$$

We expand this function to the whole complex plane by analytically continuing in regards to the frequency in a similar way to the self-energy described in Eq.(8). On that note, the first "physical" Riemann sheet of the propagator can be plotted. Expanding on this idea, we turn to the inverse of the Green's function which exhibits the Green's function poles as zeroes. These points are of great importance as they can provide the full microscopic picture of the interaction.

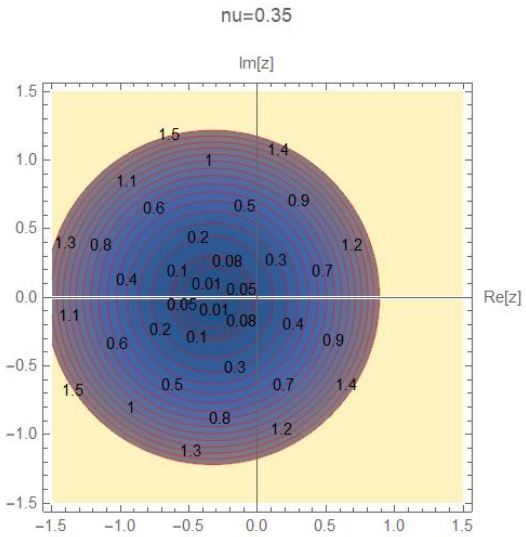

Figure 4: Example of the absolute value of the inverse propagator $G^{-1}(k,z)$ for $\nu_k = 0.35$ in the complex ω plane.

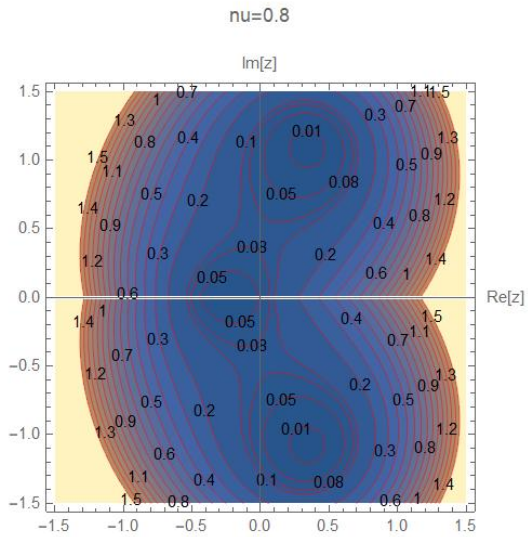

Figure 5: Example of the absolute value of the inverse propagator $G^{-1}(k,z)$ for $\nu_k = 0.8$ in the complex ω plane.

The sign of the coupling constant plays a big role in identifying these structures. Following the analysis done in the experimental side of things [5] we match the Gubser-Rocha frequency independent prefactors with the results.

$$\begin{aligned} g\ sin((\nu_k - \frac{1}{2})\pi) &= \frac{\lambda v_F}{2(\hbar\omega_N)^{2\nu_k - 1}}, \\ g\ sin((\nu_k - \frac{1}{2})\pi) &> 0. \end{aligned} \tag{11}$$

Since the coupling constant g is a renormalizable quantity we neglect its absolute value and fix its sign in accordance to the above equation. A sign change for the coupling constant is also theoretically predicted by AdS/CFT [3], which takes place at the value of $\nu_k = \frac{1}{2}$, changing from $g \propto \Gamma(\nu_k - \frac{1}{2}) = -|g|$, for $\nu_k \leq \frac{1}{2}$, to $g = |g|$, for $\nu_k \geq \frac{1}{2}$, in agreement with the above. In the $\nu_k \geq \frac{1}{2}$ case two poles appear in the first and forth quadrant of the complex plane fact that will prove to be troublesome in giving physical context to our calculations. Similar poles have been observed in Green's function calculations derived from AdS/CFT correspondence [10] that hint towards particle anti-particle symmetry violation.

2.2 Spectral function and sum-rule

The spectral function is a continuous function lying in the real axis of the analytically continued Green's function $G(k,z)$. Approaching the real axis from above we find the retarded Green's function whose self-energy has been already calculated in Eqs.(7). Hence,

$$G_R(k,\omega) = \frac{1}{\omega - c_k - g(\omega|\omega|^{2\nu_k-1}cos((\nu_k-\frac{1}{2})\pi) - i|\omega|^{2\nu_k}sin((\nu_k-\frac{1}{2})\pi))}. \tag{12}$$

Where we have set $c_k = \frac{\varepsilon_k-\mu}{\hbar}$ for notational simplicity.

In the case of a non-interacting Green's function with a small positive imaginary part added to the frequency the imaginary part of the Green's function is found as

$$\begin{aligned} Im[\lim_{\varepsilon\to 0^+} G_0(x+i\varepsilon)] &= Im[\lim_{\varepsilon\to 0^+}\frac{1}{x+i\varepsilon}] \\ &= -\lim_{\varepsilon\to 0^+}\frac{\varepsilon}{x^2+\varepsilon^2} = -\pi\delta(x), \end{aligned} \tag{13}$$

The sharp peak in the imaginary part is an indication of an existing particle thus in the free particle case this quantity is associated with the spectral function. Including the Gubser-Rocha self-energy produces a spectral function $\rho(k,\omega)$ equal to

$$\begin{aligned} \rho(k,\omega) &= -\frac{Im(G_R(k,\omega))}{\pi} \\ &= \frac{1}{\pi}\frac{g|\omega|^{2\nu_k}sin((\nu_k-\frac{1}{2})\pi)}{[\omega - c - g\omega|\omega|^{2\nu_k-1}cos((\nu_k-\frac{1}{2}\pi))]^2 + [g|\omega|^{2\nu_k}sin((\nu_k-\frac{1}{2})\pi)]]^2}. \end{aligned} \tag{14}$$

This function should obey the Riemann-Lebesgue lemma approaching zero as the frequency ω tends to infinity with a factor of $\frac{1}{\omega}$. Conventionally, this relation is verified by the sum rule [7] where the spectral function is required to equate to unity when integrated over all frequency space. At first glance, the spectral function of Eq.(14) is given in regards to the critical exponent ν_k where for $\nu_k \leq \frac{1}{2}$ it takes negative values and only for $\nu_k \geq \frac{1}{2}$ the spectral function becomes positive. This unphysical result can be easily traced back to the coupling constant g which has a sign change threshold at $\nu_k = \frac{1}{2}$, as mentioned before. The spectral function can now be plotted having shape similar to that of holographic spectral functions for varying critical exponents [8], as shown in Fig.(6).

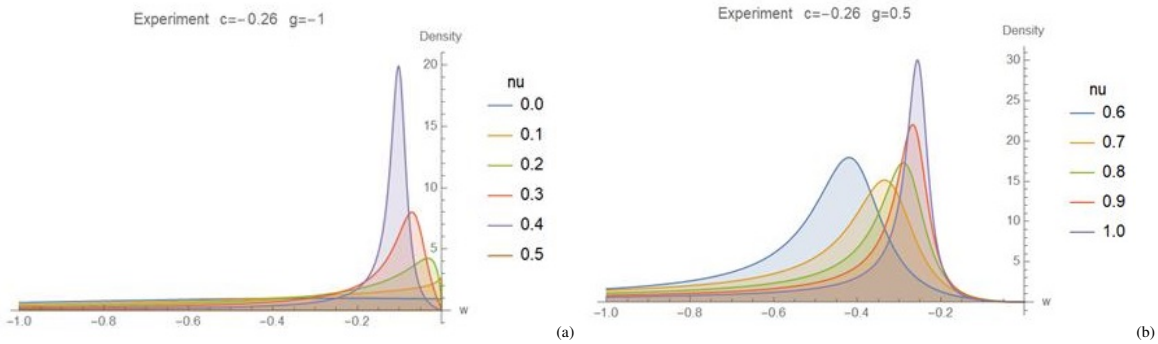

Figure 6: Spectral function plotted against frequency for values of $\nu_k \leq \frac{1}{2}$ (a) and $\nu_k \geq \frac{1}{2}$ (b).

Applying the aforementioned function to the sum-rule relation should hypothetically yield

$$\begin{aligned} 1 &= \int_{-\infty}^{\infty} d\omega \rho(\omega,k) \\ &= \int_{-\infty}^{\infty} d\omega \frac{1}{\pi} \frac{g|\omega|^{2\nu_k} sin((\nu_k - \frac{1}{2})\pi)}{[\omega - c - g\omega|\omega|^{2\nu_k - 1} cos((\nu_k - \frac{1}{2}\pi))]^2 + [g|\omega|^{2\nu_k} sin((\nu_k - \frac{1}{2})\pi)]]^2}. \end{aligned} \tag{15}$$

As mentioned in the previous section, this property of quantum mechanical spectral functions is responsible for maintaining the sum of probabilities to be equal to one.

2.3 Case: $\nu_k < \frac{1}{2}$

In this range for the critical exponent ν_k, no poles appear in the first physical sheet of the propagator. The analyticity of the Green's function in the upper complex plane, which by definition produces the aforementioned sum rule, will now work as a verifying mechanism. Integrating the analytically continued $G(z)$ along an anti-clockwise directed curve, entrapping the whole upper complex curve, yields zero as there are no poles present. So,

$$\oint_C G(z)dz = 0. \tag{16}$$

Considering the contour as a sum of a straight line on the real axis and an arc with opposing directions, this integral can be split into two. The straight integral passes through the real axis while the arc circles around the real pole on the negative real axis as shown in Fig.(4). We rewrite the contour integral as

$$\oint_{straight} G(z)dz + \oint_{arc} G(z)dz = 0. \tag{17}$$

This relation requires the imaginary part of the resulting integration to tend to zero as well. The straight line integral can be approximated by taking small positive imaginary values of z and results in an integration of the spectral function as seen before in Eq.(15). The arc integral contributes a term equal to πi since it covers only half a circle. Now we can identify this straight line integration of the imaginary part of the Green's function with the spectral function using the first equation of Eq.(14). This results in the aforementioned sum-rule

$$\int_{-\infty}^{\infty} \rho(x)dx = 1. \tag{18}$$

2.4 Case: $\nu_k > \frac{1}{2}$

These values for the critical exponent hold special value as they match the ones in our experimental reference. In this section we attempt to mend the analytical misbehaviour of the spectral function and break down its properties in this range.

Taking a closer look at the zeroes of the retarded Green's function denominator, the existence of more than one pole is prohibited for values of $\nu_k \leq 1$.

$$\omega_c = c_k + g(\omega_c|\omega_c|^{2\nu_k-1}cos((\nu_k - \frac{1}{2})\pi) - i|\omega_c|^{2\nu_k}sin((\nu_k - \frac{1}{2})\pi))$$

The apparent first and forth quadrant poles are connected with the logarithmic function used to describe the self-energy of Eq.(4). The multi-valued exponent $(\nu_k - \frac{1}{2})ln(-\omega^2 - i\varepsilon\omega)$ in the self-energy creates an infinite amount of poles scattered around the infinite Riemann sheets the same way that a function of the form $\frac{1}{e^{ix}+1}$ would [9]. These points are considered poles of first order which ruin the upper complex plane analyticity of the propagator. In the previous section this property of the Green's function was used to verify the sum rule. Yet, a single pole can still be found approximatively for the above equation. We use the Lagrange inversion theorem in order to extract a momentum dependent critical frequency following the inversion relations

$$\begin{aligned}
c_k &= f(\omega_c) = \omega_c - \Sigma(\omega_c, k), \\
\omega &= g(c_k) = c_k + \sum_{n=1}^{\infty} g_n \frac{(c_k - f(a))^n}{n!}, \\
g_n &= \lim_{\omega \to c_k} \frac{d^{n-1}}{d\omega_c^{n-1}} (\frac{\omega_c - c_k}{f(\omega_c) - f(c_k)})^n,
\end{aligned}$$

where $g_1 = 1$, as $lim_{\omega \to c_k}[\Sigma(\omega,k) - \Sigma(c_k,k)]$ tends to zero faster than $lim_{\omega \to c_k}[\omega - c_k]$ for $\nu_k \geq \frac{1}{2}$. The first order approximation is now calculated as

$$\omega_c = c_k + \Sigma(c_k,k) = c_k + g(c_k|c_k|^{2\nu_k - 1} cos((\nu_k - \frac{1}{2})\pi) - i|c_k|^{2\nu_k} sin((\nu_k - \frac{1}{2})\pi)). \tag{19}$$

Similarly to other AdS/CFT motivated papers [10] we consider terms of $c_k = \frac{\varepsilon_k - \mu}{\hbar} \propto k - k_F$ up to and including powers of $2\nu_k$ for $\frac{1}{2} \leq \nu_k$. This approximation, shown in Eq.(19), can succeed in finding the pole's location on the complex plane only for small values of c_k

In order to see how this approximation can create poles in the denominator of the retarded Green's function we apply the equation above to the corresponding denominator to find

$$\begin{aligned}
&\omega_c - c_k - g|\omega_c|^{2\nu_k}(sing(\omega_c)cos((\nu_k - \tfrac{1}{2})\pi) - isin((\nu_k - \tfrac{1}{2})\pi)) = \\
&g|c_k|^{2\nu_k}(sign(c_k)cos((\nu_k - \tfrac{1}{2})\pi) - isin((\nu_k - \tfrac{1}{2})\pi)) + \cancel{c_k} - \cancel{c_k} \\
&- g|c_k + g(c_k|c_k|^{2\nu_k - 1}cos((\nu_k - \tfrac{1}{2})\pi) - i|c_k|^{2\nu_k}sin((\nu_k - \tfrac{1}{2})\pi))|^{2\nu_k}(sign(\omega_c)cos((\nu_k - \tfrac{1}{2})\pi) - isin((\nu_k - \tfrac{1}{2})\pi)) \\
&= g|c_k|^{2\nu_k}(sign(c_k)cos((\nu_k - \tfrac{1}{2})\pi) - isin((\nu_k - \tfrac{1}{2})\pi)) - g|c_k|^{2\nu_k}(sign(\omega_k)cos((\nu_k - \tfrac{1}{2})\pi) - isin((\nu_k - \tfrac{1}{2})\pi)) + O(c_k^{2\nu_k + 1}) \\
&\approx 0, \quad \text{for sign}(\omega_c) = \text{sign}(c_k).
\end{aligned}$$

To perform the calculations described above we have used the fact that the factor $|\omega_c|^{2\nu_k}$ expands into terms with powers of c_k bigger than $2\nu_k$ which are simplified for $\frac{1}{2} \leq \nu_k$ leaving just the term $|c_k|^{2\nu_k}$. The sign of the critical frequency is considered to be the same as the sign of c_k while in the case that these two quantities have a different sign the pole approximation

$$\omega_c = c_k + g(-c_k|c_k|^{2\nu_k - 1}cos((\nu_k - \frac{1}{2})\pi) - i|c_k|^{2\nu_k}sin((\nu_k - \frac{1}{2})\pi)),$$

can be used to get the same outcome. Now we turn again to the sum rule where the integration over frequencies has to be done along the upper-half complex plane as discussed before. For this reason we choose the conjugate of the pole found previously since it lies in our area of interest and is also a valid pole of the spectral function. In order to perform the contour integral on the complex plane, we split the anti-clockwise contour C that engulfs the upper-half plane into two parts. The first one is $C_{straight}$ which accounts for the integration along the real axis and the second one is C_{Arc} whose contribution to the integral vanishes as we get to bigger ω. Thus, the straight line is

exactly equal to the contour integral along C

$$\begin{aligned}
&\oint_C d\omega \frac{1}{\pi} g|\omega|^{2\nu_k} sin((\nu_k - \frac{1}{2})\pi) \frac{1}{\omega - c_k - g\omega|\omega|^{2\nu_k - 1} cos((\nu_k - \frac{1}{2})\pi) + ig|\omega|^{2\nu_k} sin((\nu_k \frac{1}{2})\pi))} \\
&\frac{1}{\omega - c_k - g\omega|\omega|^{2\nu_k - 1} cos((\nu_k - \frac{1}{2})\pi) - ig|\omega|^{2\nu_k} sin((\nu_k \frac{1}{2})\pi))} \\
&= 2\pi i Res \left[\frac{1}{\pi} \frac{g|\omega|^{2\nu_k} sin((\nu_k - \frac{1}{2})\pi)}{\omega - c_k - g\omega|\omega|^{2\nu_k - 1} cos((\nu_k - \frac{1}{2})\pi) + ig|\omega|^{2\nu_k} sin((\nu_k \frac{1}{2})\pi))} \right]_{\omega = \omega_c^*} \\
&\approx 2\pi i (\frac{1}{\pi} \frac{g|c_k|^{2\nu_k} sin((\nu_k - \frac{1}{2})\pi)}{2ig|c_k|^{2\nu_k} sin((\nu_k - \frac{1}{2})\pi)}) \\
&= 1.
\end{aligned} \tag{20}$$

This process has normalized the spectral function approximatively so the sum of all probabilities amount to unity. To further our calculation's accuracy, we turn to second-order approximation of the pole calculated in the previous segment. The second-order approximation is also considered where we keep terms of c_k up to the $4\nu_k$ order. So,

$$\begin{aligned}
\omega_{c2} = c_k - g(c_k^2 + 2g|c^{2\nu_k+1}|cos((\nu_k - \frac{1}{2})\pi) + g^2|c_k^{4\nu_k}|)^{\nu_k} cos((\nu_k - \frac{1}{2})\pi) \\
- ig(c_k^2 + 2g|c^{2\nu_k+1}|cos((\nu_k - \frac{1}{2})\pi) + g^2|c_k^{4\nu_k}|)^{\nu_k} sin((\nu_k - \frac{1}{2})\pi).
\end{aligned}$$

In order to provide an additional evaluation criteria for the above approximations we transform these complex poles into Lorentzian distributions and compare the results. In this scenario two different parameters play roles of great importance. The first is the position of the maxima in between cases, given by the real part of the pole, and secondly the width of the Lorentzian dictated by the imaginary part of the pole. Since the matching done in [5] is valid for momenta close to the Fermi momenta, where $\frac{-0.26}{\hbar} eV \leq c_k$ we expect the validity of the pole approximations to become apparent in a similar region of energies.

Taking a glance at Fig.(7) the approximations show high dependence on the coupling constant g, where smaller values of it lead to a better agreement with the experiment. This fact will be taken into account when deriving results based on this approximation. More than that, the c_k parameter has been tuned at the least favourable value of $\frac{-0.26}{\hbar}$ where closer to zero values lead to a better result.

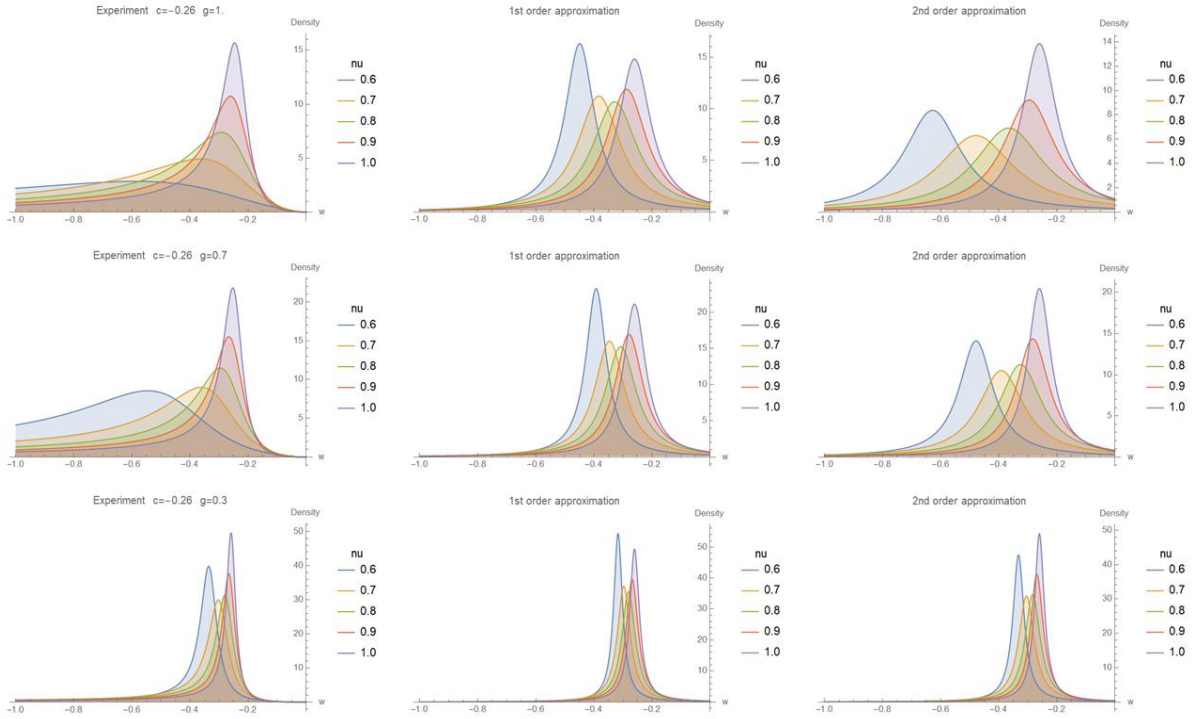

Figure 7: Lorentzian approximations of first (ω_c) and second (ω_{c2}) order for varying values of coupling constant g and $c = -0.26$.

Alternatively we can separate the spectral function into two components its width and the position where it takes its maximum value. Given the fact the non-interactive spectral function is considered to be equal to a delta function, we study the range where the above approximation stands true. Following a local optimization fit the width of the spectral function is plotted in Fig.(8), where the ratio of the Lorentzian's height, being equal to $\frac{2}{\pi\Gamma}$, over width was also used to separate the graph into regions where the claim of a delta-like spectral function is most prevalent. We extract the momentum dependence of the width by taking different values of c_k and ν_k separately inside the experimental range which were later combined to get the behaviour of the width in regards to doping. More than that the spectral function maximum can be approximated following the same procedure shown in Fig.(9). It is inherent to the power law relation of the self-energy that the largest standard error appears near the edge values of the critical exponent. Taking that into account and a five-fold height to width ratio, the delta function approximation is thought to be valid for the range $0.6 \leq \nu_k \leq 1$.

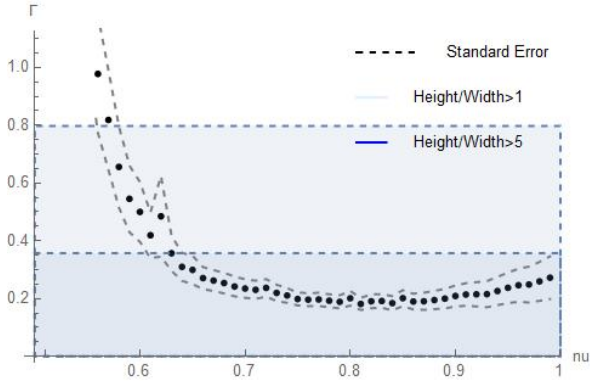

Figure 8: Numerical fit of the width of spectral function in the experimental range.

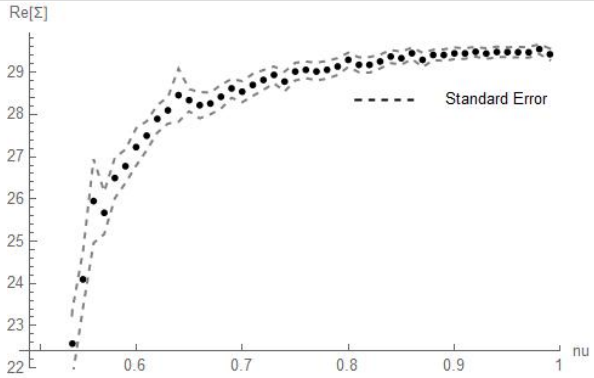

Figure 9: Numerical fit of the real part of the self-energy in the range $\frac{1}{2} \leq \nu_k \leq 1$.

Considering that the power law nature of the self-energy becomes troublesome for the Green's function's analyticity and poses great obstacles in further calculations we approximate its behaviour by a function of the form

$$\omega|\omega|^{2\nu_k-1}cos((\nu_k-\frac{1}{2})\pi) \rightarrow [a+b(\nu_k-1)+c(\nu_k-1)^2]\omega+[d+f(\nu_k-\frac{1}{2})+l(\nu_k-\frac{1}{2})^2]\omega^2.$$

Table 1: Fitting parameters for Re[Σ]

	Linear dependence		Quadratic dependence
a	0.185986	d	0.0469406
b	-0.643364	f	0.222502
c	3.28174	l	7.7821

Since the critical exponent has been restricted to values that make the self-energy relation linear or quadratic, higher powers of frequency dependence do not lead to

better approximations. It is also worth mentioning that a greater weight has been put on lower values of ω which contribute most for momentum values close to the Fermi surface. The fitted equation can be now put to the test by comparing the function to the original as shown in Fig.(10) where a good agreement is found up to the critical exponent value of 0.9. This numerical approximation, in contrast with the original form, can allow us to extract the momentum dependence of the real part of the self energy as a factor since the critical exponent does not appear as a power order of frequency.

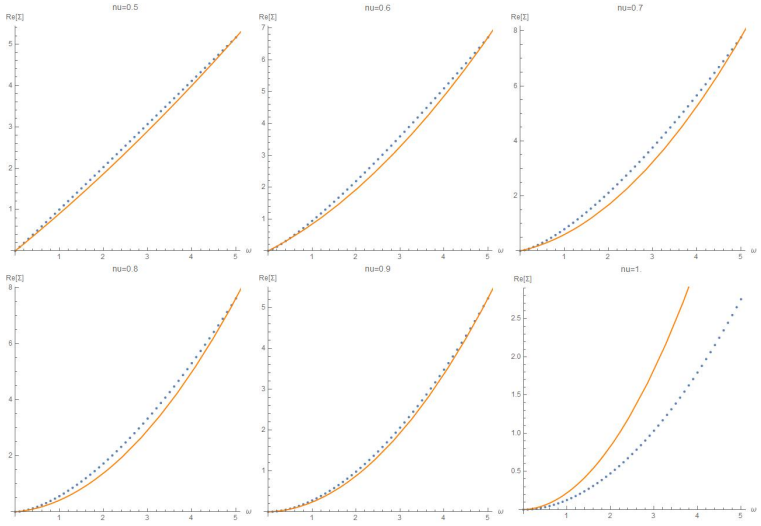

Figure 10: Fitted function of $Re[\Sigma]$, plotted as the orange curve, compared against the original, plotted with blue dots.

2.5 Analytic structure of the second Riemann sheet

In this section we study the analytical structure of the propagator outside the first, physical Riemann sheet. The points of most interest are its poles where a classification of them according to their characteristic features can provide information about unstable particles. The propagator poles which are of most interest appear for $Im(\omega) < 0$ and $Re(\omega) > 0$ and are called resonances [11]. The second Riemann sheet can found by analytically continuing the Green's function[12](or the inverse of it) below the branch cut in a way that

$$G^{(2)}(x - i\varepsilon) = G^{(1)}(x + i\varepsilon). \tag{21}$$

The superscript in this case is used for noting the first and second Riemann sheets Since the discontinuity around the branch cut is defined by

$$G^{(1)}(x+i\varepsilon) - G^{(1)}(x-i\varepsilon) = 2\pi i\rho(x), \tag{22}$$

where ρ the spectral function. The merging of the upper complex physical plane and lower unphysical plane should be done in a continuous manner. The identity theorem states that if two given functions f and g, both holomorphic on a domain Ω, equal each other on some line segment U lying in Ω, then they equal each other on the whole domain Ω [13]. This means that we can analytically continue the inverse propagator function as $\omega = z = x + yi$ analytically from the upper-half complex plane to the lower-half second Riemann sheet. Given the fact the quantity of interest is the inverse of the Green's function, we define $\sigma(x)$ as the inverse of the retarded Green's function minus the inverse advanced Green's function. This allows us to rewrite Eq.(22) as

$$G^{(2)}(z)^{-1} = G^{(1)}(z)^{-1} + 2\pi i\sigma(z) \tag{23}$$

$$\sigma(z) = -\frac{Im[G^{(1)}(z)^{-1}]}{\pi}, \tag{24}$$

where $\sigma(x)$ is analytically continued to the whole complex plane. Borrowing the Green's function form, from section 1, we apply this process in a similar manner to [13] [14][15]. The second Riemann sheet propagator, which is continuous across the real axis, can now be evaluated by the sum of the physical Green's function and the inverted spectral function's value on the real axis [12]. This process results in deforming the branch cut in a way that the pole hiding behind it can be revealed. Taking the inverse propagator relation for the whole complex plane yields:

$$G^{(2)}(z)^{-1} = G^{(1)}(z)^{-1} + 2i\mathrm{Im}[(G^{(1)}(z))^{-1}].$$

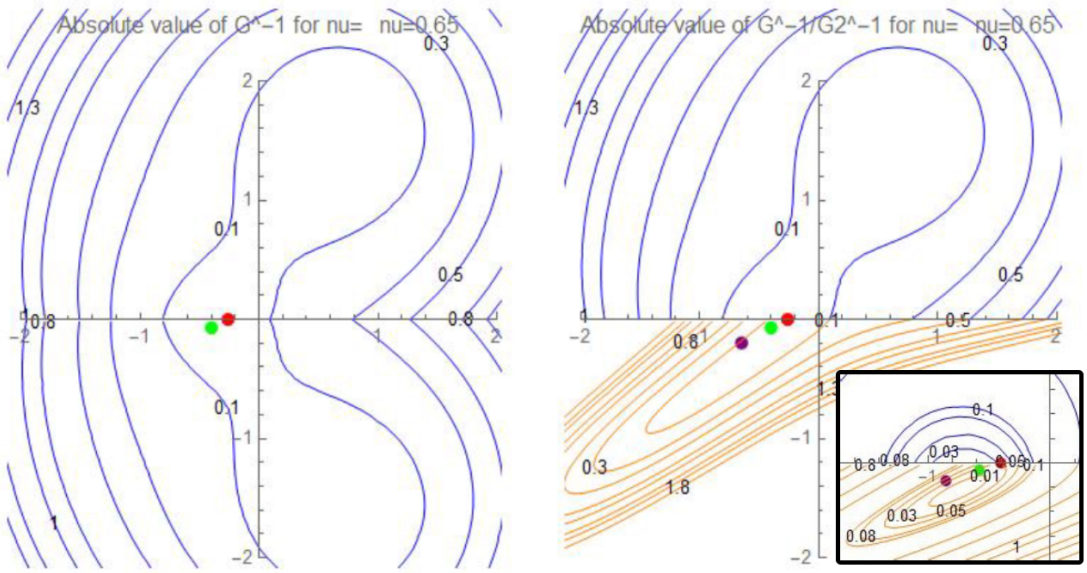

Figure 11: (a) The first physical sheet of the inverse propagator where c_k is identified as the red dot and the pole approximation of Eq.(19) with the green one. (b) The first sheet of the inverse propagator on the upper half plane matched with the second Riemann sheet of the inverse propagator for the lower complex plane. An additional purple dot signifies the second order approximation of the pole.

The second Riemann sheet can is now plotted in Fig.(11) and searched for complex poles. The approximative relation of Eq.(19) was also indicated on the complex plane which seems to track a pole underneath the branch cut next to the negative real axis. An important detail for this process is that we are expanding the upper complex plane onto the lower without passing any branch cuts, so the angle of the complex self-energy remains similar to that of the retarded Green's function of Eq.(12) instead of the advanced one. This threat to our function's analyticity is inherit to the rational nature of the critical exponent and is present in all the infinite logarithmic sheets of the propagator.

Hubbard–Stratonovich transformation and ladder-diagram calculations

The Hubbard-Stratonovich transformation is a manipulation of the system's action where a new collective field is added in a way that decouples the interaction terms between fermionic fields. This allows for a simplified theoretical description of the system where the fermionic fields can be integrated out, as described later in the text. Through this transformation useful quantities can be determined that will later lead to the calculation of observable quantities like the critical temperature of the phase transition or the coherence length of the condensate [16]. We initialize this model by considering the non interacting case of a many particle Lagrangian inside the action functional, which yields

$$\begin{aligned} S_0[\mathscr{L}[\phi^*,\phi]] &= \sum_a \int_0^{\hbar\beta} d\tau \int dx \mathscr{L}[\phi_a^*(x,\tau),\phi_a(x,\tau)] \\ &= \sum_a \int_0^{\hbar\beta} d\tau \int dx \phi_a^*(x,\tau)(\hbar\frac{d}{d\tau} - \frac{\hbar^2\nabla^2}{2m} + \varepsilon_a - \mu)\phi_a(x,\tau), \end{aligned} \tag{25}$$

where we denote ε_a as the Hamiltonian eigenvalues and μ as the chemical potential.

3.1 Matsubara Expansion

We attempt to simplify the action by Fourier transforming the electron fields in a similar manner to that of a Matsubara expansion

$$\phi_a = \sum_{\mathbf{n}} \sum_n \phi_{\mathbf{n},n,a} \chi_{\mathbf{n}}(x) \frac{e^{-i\omega_n\tau}}{\sqrt{\hbar\beta}}, \tag{26}$$

where $\beta = \frac{1}{k_B T}$ and k_B the Boltzmann constant. In this case, the imaginary frequency space is written in regards to the Matsubara frequencies, where $\omega_n = \frac{\pi n}{\hbar\beta}$ for bosons and $\omega_n = \frac{\pi(2n+1)}{\hbar\beta}$ for fermions. The action is now transformed in a way that our operators can take their corresponding eigenvalues

$$\begin{aligned} S[\phi^*,\phi] &= \sum_{a,a'} \int_0^{\hbar\beta} d\tau \int dx \sum_{\mathbf{n},n} \sum_{\mathbf{n}',n'} \phi_{\mathbf{n},n,a} \chi_{\mathbf{n}}^*(x) \frac{e^{i\omega_n\tau}}{\sqrt{\hbar\beta}} (\hbar\frac{d}{d\tau} - \frac{\hbar^2\nabla^2}{2m} + \varepsilon_{a,a'} - \mu)\phi_{\mathbf{n}',n',a'} \chi_{\mathbf{n}'}(x) \frac{e^{-i\omega_n\tau}}{\sqrt{\hbar\beta}} \\ &= \sum_{a,a'} \int_0^{\hbar\beta} d\tau \int dx \sum_{\mathbf{n},n} \sum_{\mathbf{n}',n'} \phi_{\mathbf{n},n,a}^* \chi_n^*(x) \frac{e^{i\omega_n\tau}}{\sqrt{\hbar\beta}} (-\hbar\omega_{n'} + \varepsilon_{\mathbf{n}'} + \varepsilon_{a,a'} - \mu)\phi_{\mathbf{n}',n',a'} \chi_{\mathbf{n}'}(x) \frac{e^{-i\omega_{n'}\tau}}{\sqrt{\hbar\beta}}, \end{aligned} \tag{27}$$

where $\varepsilon_{\mathbf{n}'}$ is the eigenenergy of the $\mathbf{n}'$th Matsubara frequency and $\varepsilon_{a,a'}$ the eigenenergy corresponding to spin. Using that $\int_0^{\hbar\beta} d\tau \frac{e^{i(\omega_{\mathbf{n}}-\omega_{\mathbf{n}'})\tau}}{\hbar\beta} = \delta_{\mathbf{n},\mathbf{n}'}$ the above expression can be simplified to

$$S[\phi^*,\phi] = \sum_{\mathbf{n},n,}\sum_{a}\phi_{\mathbf{n},n,a}(-\hbar\omega_n + \varepsilon_{\mathbf{n},a} - \mu)\phi_{\mathbf{n},n,a}, \tag{28}$$

where we denote the total energy by $\varepsilon_{\mathbf{n},a,a'}$. We now turn to the partition function defined as

$$Z_0 = \int d[\phi^*]d[\phi] exp\{-\frac{1}{\hbar}\sum_{a,a'}\int_0^{\hbar\beta} d\tau \int_0^{\hbar\beta} d\tau' \int dx \int dx' \phi_a(x,\tau)^* G^{-1}_{0;a,a'}(x,\tau;x',\tau')\phi_a(x',\tau')\}. \tag{29}$$

The Green's function G is the solution when the Lagrangian operator is applied on the fields and can be found from solving the following equation.

$$G^{-1}_{0;a,a'}(x,\tau;x',\tau') = -\frac{1}{\hbar}(\hbar\frac{d}{d\tau} - \frac{\hbar^2\nabla^2}{2m} + \varepsilon_{a,a'} - \mu)\delta(x-x')\delta(\tau-\tau'). \tag{30}$$

Expanding it in the same way as before for discrete states we can extract the momentum representation of the Green's function from inside the Fourier transform.

$$G_{0;a,a'}(x,\tau;x',\tau') = \sum_{\mathbf{n},n}\frac{-\hbar}{-i\hbar\omega_n + \varepsilon_{\mathbf{n},a,a'} - \mu}\chi_{\mathbf{n}}(x)\chi_{\mathbf{n}}*(x')\frac{e^{-i\omega_n(\tau-\tau')}}{\hbar\beta}, \tag{31}$$

where in momentum space

$$G_{0;a,a'}(\mathbf{n},n;\mathbf{n}',n') = \delta_{\mathbf{n},\mathbf{n}'}\delta_{n,n'}\frac{-\hbar}{-i\hbar\omega_n + \varepsilon_{\mathbf{n},a,a'} - \mu}. \tag{32}$$

Now the integration of the fermionic fields is made possible by the identity:

$$\begin{aligned} Z &= \int [d\phi^*]d[\phi] exp\{(\phi|G^{-1}|\phi) + (J|\phi) + (\phi|J)\} \\ &= exp\{\mp Tr[log(-G^{-1})], \end{aligned} \tag{33}$$

where $((\phi|G^{-1}|\phi))$ representing the action and J the added sources [16]. Specifically:

$$\begin{aligned} Z_0 &= \int (\Pi_{\mathbf{n},n,a} d\phi^*_{\mathbf{n},n,a} d\phi_{\mathbf{n},n,a} \frac{1}{(2\pi i)^{\frac{1\pm1}{2}}}\frac{1}{(\hbar\beta)^{\pm1}}) exp\{-\frac{1}{\hbar}\sum_{\mathbf{n},n,a}\phi^*_{\mathbf{n},n,a}(-i\hbar\omega_n + \varepsilon_{\mathbf{n},a} - \mu)\phi_{\mathbf{n},n,a}\} \\ &= exp\{\mp\sum_{\mathbf{n},n,a} ln(\beta(-i\hbar\omega_n + \varepsilon_{\mathbf{n},a} - \mu))\}, \end{aligned} \tag{34}$$

where the term $\frac{1}{(\hbar\beta)^{\pm 1}}$ comes from the Jacobian of the wavefunction integration, as we transform the field ϕ_a to its momentum space equivalent $\phi_{\mathbf{n},n,a}$. Taking a closer look at the sum in the exponent and narrowing our focus to the frequency index n, we notice that the discrete summation can be turned into complex integration by analytically continuing the frequency space [16][17].

$$\frac{1}{\hbar\beta}\sum_n ln(-i\hbar\omega_n+\varepsilon-\mu)=\frac{1}{2\pi i}\oint_C ln(-\hbar z+\varepsilon-\mu). \tag{35}$$

It is essential for the contour C to contain no divergences like the one created by the logarithmic function presented at Sec.(2.1). For values of $\frac{\varepsilon-\mu}{\hbar} < z$ the contour is deformed and partitioned into C, C' and C'', as shown in Fig.(12), so that the branch-cut is avoided. The Matsubara poles can be now elegantly added by multiplying by the quantity $lim_{\eta\to 0}\frac{\pm\hbar\beta e^{\eta z}}{e^{\beta\hbar z}\mp 1}$. This term is made so its contribution, when performing the contour integration, to be equal to ± 1, with -1 corresponding to fermions and $+1$ to bosons. Its poles are simple and, considering that $z=i\omega_n$, they correspond to the odd and even Matsubara frequencies. The importance of this addition can be readily seen by identifying the additional term with the Fermi-Dirac or Bose-Einstein distribution for fermions and bosons respectively. Since the total contour is made to enclose no poles, the complex integration yields zero

$$lim_{\eta\to 0}\frac{1}{2\pi i}\oint_{C+C'+C''} ln(-\hbar z+\varepsilon-\mu)\frac{\pm e^{\eta z}}{e^{\hbar\beta z}\mp 1}=0.$$

The contour of interest C is now calculatable as a function of the rest of the contours. The contour C' gives no contribution when integrated over.

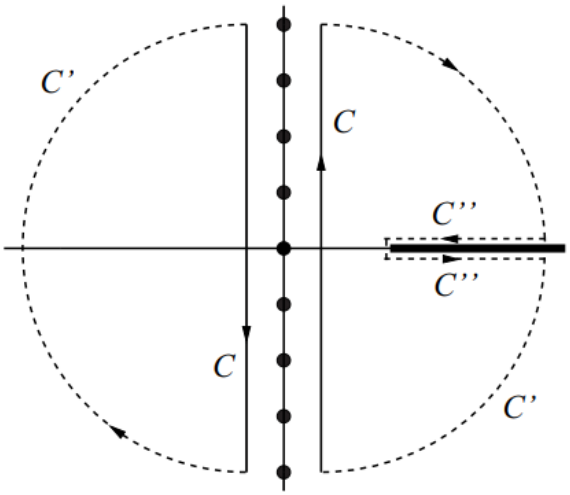

Figure 12: Contour in complex plane avoiding the Matsubara poles on the imaginary axis and the real pole on the real axis [16].

This can be readily seen, if one considers that the Green's functions should converge to zero, for high frequency modes, with a convergence ratio of $\frac{1}{\omega}$, fact which is made sure by the sum rule Eq.(15). So

$$lim_{\eta\to 0}\frac{1}{2\pi i}\oint_C ln(-\hbar z+\varepsilon-\mu)\frac{\pm e^{\eta z}}{e^{\hbar\beta z}\mp 1} = lim_{\eta\to 0}\frac{1}{2\pi i}\oint_{C''} ln(-\hbar z+\varepsilon-\mu)\frac{\mp e^{\eta z}}{e^{\hbar\beta z}\mp 1}$$
$$= \int_{\frac{\varepsilon-\mu}{\hbar}}^{\infty} dz\frac{\mp 1}{e^{\hbar\beta z}\mp 1} = \mp[z-\frac{ln(e^{\hbar\beta z}\pm 1)}{\hbar\beta}]_{z=\frac{\varepsilon-\mu}{\hbar}}^{\infty} = \mp\frac{1}{\hbar\beta}ln(\frac{e^{\beta(\varepsilon-\mu)}}{e^{\beta(\varepsilon-\mu)}\pm 1}). \tag{36}$$

This is the process we will attempt to recreate with the addition of interactions like the self-energy described before.

3.2 Introducing the self-energy

In the case of self-energy contributions the particle is considered to interact and so the action now attains a new interaction term.

$$Z = \int d[\phi^*]d[\phi]exp\{-\frac{S_0[\phi^*,\phi]+S_{int}[\phi^*,\phi]}{\hbar}\} \tag{37}$$

To implement this interaction into the non-interacting system we expand the exponential with the interaction term. In order to do that first we must consider an interaction which is weak, so the series expansion of the exponential function makes sense for lower order terms. The Green's function can now be written as a correlation function including the non-interacting Green's functions as

$$< \phi(x,\tau)\phi^*(x',\tau')S_{int}[\phi,\phi^*] > . \tag{38}$$

Applying Wick's theorem on the aforementioned terms we notice that an interaction involving different spin states between particles produces terms with three different spin indices making the outcome null. That is the reason this interaction has been considered diagonal is spin space similar to the Green's function terms. Turning to momentum space the interactive part of the action is renamed as self-energy and the propagator is now described by the following equation

$$G_a(k,i\omega_n) = G_{0;a}(k,i\omega_n) + G_{0;a}(k,i\omega_n)\Sigma(k,i\omega_n)G_a(k,i\omega_n). \tag{39}$$

Multiplying by the right with G^{-1} and from the left with $G_{0;a}^{-1}$ yields

$$G_a^{-1}(k,i\omega_n) = G_{0;a}^{-1}(k,i\omega_n) - \Sigma(k,i\omega_n). \tag{40}$$

We can depict this expansion called Dyson series with Feymann diagrams. The first order expansion of the propagator is then considered as

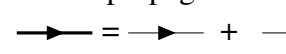

where the thick line corresponds to the interacting propagator while the thin one to the non-interacting one. This comes as no surprise as we have studied the Gubser-Rocha self-energy using this process in the previous section. The contribution of the interaction can be seen as a shift in the pole location of the non-interacting Green's function. From now on this corrected Green's function will be noted as $G_{GR}(k,\omega_n)$.

3.3 Hubbard-Stratonovich

Considering a general form of fourth-order interaction between fields we can start molding the case of an attractive interaction between fermions that can lead to a phase transition

$$\begin{aligned} V_{int} &= \frac{1}{2}\int_0^{\hbar\beta} d\tau \int dx \int dx' \phi_\uparrow^*(x,\tau)\phi_\downarrow^*(x,\tau)V(x-x')\phi_\uparrow(x',\tau)\phi_\downarrow(x',\tau), \\ Z &= \int d[\phi^*]d[\phi] exp\{-\frac{S_0[\phi^*,\phi]+S_{int}[\phi^*,\phi]+V_{int}[\phi^*,\phi]}{\hbar}\}, \\ V(x-x') &= V_0\delta(x-x'). \end{aligned} \tag{41}$$

We can incorporate such an interaction into the previous model by adding a new collective field, without changing the rest of the system

$$\int d[\Delta^*]d[\Delta] exp\{\frac{1}{2\hbar}(\Delta^* - V\phi_\uparrow^*\phi_\downarrow^*|V^{-1}|\Delta - V\phi_\uparrow\phi_\downarrow)\} = 1. \tag{42}$$

The importance of such transformation is apparent when taking a closer look at the fourth-order term which can be made, in the case of Hubbard-Stratonovich transformations, to eliminate any other fourth-order interaction term when multiplied with the partition function

$$\int d[\Delta^*]d[\Delta] exp\{(V\phi_\uparrow^*\phi_\downarrow^*|V^{-1}|V\phi_\uparrow\phi_\downarrow)\}. \tag{43}$$

Introducing this transformation on the partition function yields

$$\begin{aligned} Z = \int d[\phi*]d[\phi] \int d[\Delta^*]d[\Delta] exp\{-\sum_{a=\uparrow,\downarrow}\int_0^{\hbar\beta}\int dx \frac{|\Delta(x,\tau)|^2}{V} - \hbar\int_0^{\hbar\beta} d\tau \int dx \int_0^{\hbar\beta} d\tau' \int dx' \phi_a^*(x,\tau)G_{0;a}^{-1}\phi_a(x',\tau') \\ + \int_0^{\hbar\beta} d\tau \int dx \int_0^{\hbar\beta} d\tau' \int dx' (\phi_\uparrow^*(x,\tau)\phi_\downarrow^*(x,\tau)\Delta(x,\tau) + \Delta^*(x,\tau)\phi_\uparrow(x,\tau)\phi_\downarrow(x,\tau))\}. \end{aligned} \tag{44}$$

This interaction between the newly added field and the old one is the only trade off for removing the forth-order interaction. The next step is to incorporate the second and third term from the above equation in a way that a new interacting Green's function can arise

$$\begin{aligned} Z = \int d[\phi*]d[\phi] \int d[\Delta^*]d[\Delta] exp\{ - \sum_{a=\uparrow,\downarrow} \int_0^{\hbar\beta} \int dx \frac{|\Delta(x,\tau)|^2}{V} \\ - \hbar \int_0^{\hbar\beta} d\tau \int dx \int_0^{\hbar\beta} d\tau' \int dx' [\phi^*_\uparrow(x,\tau)\phi_\downarrow(x,\tau)] G_a^{-1} \begin{bmatrix} \phi_\uparrow(x',\tau') \\ \phi^*_\downarrow(x',\tau') \end{bmatrix} \}. \end{aligned} \tag{45}$$

For now the collective field will simply play the role of a theoretical tool that can guide us through the formalism. The most practical equation that we can extract so far is that of the total Green's function with both self-energy contributions

$$\begin{aligned} G_a^{-1}(x,\tau;x',\tau') = G^{-1}_{GR;a}(x,\tau;x',\tau') - \Sigma(x,\tau;x',\tau') = \\ \begin{bmatrix} G^{-1}_{0;\uparrow}(x,\tau;x',\tau') - \Sigma_{1,1}(x,\tau;x',\tau') & \Sigma_{1,2}(x,\tau;x',\tau') \\ \Sigma_{2,1}(x,\tau;x',\tau') & -G^{-1}_{0;\downarrow}(x,\tau;x',\tau') - \Sigma_{2,2}(x,\tau;x',\tau') \end{bmatrix}. \end{aligned} \tag{46}$$

Keeping the term $g\omega(-\omega^2)^{\nu_k - \frac{1}{2}}$ from the momentum space representation of the Gubser-Rocha self-energy as a pole correction term for the Green's function diagonal elements, we turn our attention to the forth order interaction. This interaction can now become the driving force for condensation by considering it attractive and point like, meaning it is of the type $V(x-x') = V\delta(x-x')$, where $V < 0$. Its connection with the added collective field is now dictated by the following equation

$$\hbar\Sigma_{1,2}(x,\tau;x',\tau';\Delta(x,\tau)) = \delta(x-x')\delta(\tau-\tau')\Delta(x,\tau). \tag{47}$$

The Green's function is put back together where the contribution of each term is depicted in matrix notation as

$$\begin{aligned} G_a^{-1}(x,\tau;x',\tau') = G^{-1}_{GR;a}(x,\tau;x',\tau') - \Sigma(x,\tau;x',\tau') \\ = \begin{bmatrix} G^{-1}_{GR;\uparrow}(x,\tau;x',\tau') & \frac{\Delta(x,\tau)}{\hbar}\delta(x-x')\delta(\tau-\tau') \\ \frac{\Delta^*(x,\tau)}{\hbar}\delta(x-x')\delta(\tau-\tau') & -G^{-1}_{GR;\downarrow}(x,\tau;x',\tau'). \end{bmatrix} \end{aligned} \tag{48}$$

3.4 Ladder-diagram summation

Extract the Green's function from the previous subsection, we can calculate the trace of the resulting matrix from the partition function by integrating out the fermionic fields

$$Z = \int d[\Delta^*]d[\Delta] exp\{\int_0^{\hbar\beta} d\tau \int dx \frac{|\Delta(x,\tau)|^2}{V}\} exp\{Tr[log(-G_a^{-1})]\}. \tag{49}$$

So far no alteration has happened to the system, just a manipulation to the partition function so it can be written as an integral over the collective field. We can expand the logarithmic trace term in the action following a series expansion of the form

$$log(a^{-1} - b) = log(a^{-1}) + log(1 - ab) = log(a^{-1}) + \sum_{n=0}^{\infty} \frac{1}{n}(ab)^n. \tag{50}$$

Our case follows a similar path where odd powers of the index n powers result to zero. This claim comes from the fact that the resulting interacting Green's function matrix of Eq.(49) has only off-diagonal terms when raised to an odd power.

$$Tr[log(-G_a^{-1})] = Tr[log(-G_{GR}^{-1})] - \sum_{n=1}^{\infty} \frac{1}{n} Tr[(G_{GR}\Sigma)^n]]. \tag{51}$$

This collective field is shown to appear in the total action even powers. In order to study the phase transition that this system can describe first we need to identify it with the usual Landau free energy density of the type

$$\frac{S[k^*,k]}{\hbar\beta V} = f(|k|) = a(T)|\Delta|^2 + b(T)|\Delta|^4 + \dots . \tag{52}$$

The transition is defined by the $a(T)$ parameter of the free energy expansion. When this parameter switches signs the energy of the system changes its minima. It gains its first term from the residual term of the Hubbard-Stratonovich transformation and a second one from the logarithmic expansion since summing Eq.(52) in regards to n produces only even powers of the field $\Delta(x,\tau)$. We denote the second order of the expansion as $\Xi(T)$

$$\Xi(T) = \frac{\hbar}{2} Tr[(G_{GR}\Sigma)^2]. \tag{53}$$

Expanding $\Xi(T)$ into its integral form yields:

$$\Xi(T) = -\frac{1}{\hbar}\int_0^{\hbar\beta} d\tau d\tau' d\tau'' d\tau''' \int dx dx' dx'' dx''' dx' G_{GR;\uparrow}(x,\tau;x',\tau')\Sigma_{1,2}(x',\tau';x'',\tau'')G_{GR;\downarrow}(x'',\tau''';x,\tau''')\Sigma_{2,1}(x''',\tau''';x,\tau). \tag{54}$$

Since the off-diagonal self-energy has delta function proportionality, the second order expansion term can be simplified to a more convenient form.

$$\hbar\Sigma_{2,1}(x,\tau;x',\tau';\Delta(x,\tau)) = \hbar\Sigma_{1,2}(x,\tau;x',\tau';\Delta(x,\tau)) = \delta(x-x')\delta(\tau-\tau')\Delta(x,\tau), \tag{55}$$

$$\Xi(T) = -\frac{1}{\hbar}\int_0^{\hbar\beta} d\tau d\tau' \int dx dx' G_{GR;\uparrow}(x,\tau;x',\tau')k(x,\tau)G_{GR;\downarrow}(x',\tau';x,\tau)k^*(x',\tau'). \tag{56}$$

This results in an $a(T)$ parameter which is a functional of the Green's function containing the Gubser-Rocha self-energy

$$\begin{aligned} a(T) &= -\frac{1}{V_0} - \frac{1}{\hbar^2\beta}\int_0^{\hbar\beta} d\tau d\tau' \int dx dx' G_{GR;\uparrow}(x,\tau;x',\tau')G_{GR;\downarrow}(x,\tau;x',\tau') \\ &= -\frac{1}{V_0} - \frac{1}{\hbar^2\beta}\int \frac{d\mathbf{k}}{(2\pi)^2}\sum_n G_{GR;\uparrow}(\mathbf{k},i\omega_n)G_{GR;\downarrow}(\mathbf{k}'-\mathbf{k},i(\omega'-\omega_n)) \\ &= -\frac{1}{V_0} - \frac{1}{\hbar^2\beta}\int \frac{d\mathbf{k}}{(2\pi)^2}\sum_n \frac{1}{i\omega_n - \frac{\varepsilon_{\mathbf{k}}-\mu}{\hbar} - \Sigma(\mathbf{k},i\omega_n)} \frac{1}{i(\omega'-\omega_n) - \frac{\varepsilon_{\mathbf{k}'-\mathbf{k}}-\mu}{\hbar} - \Sigma(\mathbf{k}'-\mathbf{k},i(\omega'-\omega_n))}. \end{aligned} \tag{57}$$

Where V_0 is the interaction strength and the chemical potential is considered equal for different spin directions $\mu = \mu_\uparrow = \mu_\downarrow$. The complexity of the Gubser-Rocha self-energy dictates that our approach to this interacting case must be somewhat similar to the one described for the non-interacting one in order for an analytic result to be made. This self-energy is integrated over the entire range of frequencies fact that will prove to be troublesome. Since the critical exponent is momentum dependent we must consider all possible values and evidently all the possible frequency integration results which vary drastically. Its complication can be diminished by narrowing our range of interest to the case of $\omega \to 0$. It is a reasonable approximation which was already made to derive the Gubser-Rocha self-energy a priori [3]. The simplifications start from the term

$$\begin{aligned} &\Sigma(\mathbf{k}'-\mathbf{k},i(\omega'-\omega_n)) = g(\omega'-\omega_n)[-(\omega'-\omega_n)^2]^{\nu_{\mathbf{k}'-\mathbf{k}}-\frac{1}{2}} = g i^{2\nu_{\mathbf{k}'-\mathbf{k}}-1}(\omega'-\omega_n)^{2\nu_{\mathbf{k}'-\mathbf{k}}-1} \\ &= g_{\mathbf{k}'-\mathbf{k}}[(-\omega_n)^{2\nu_{\mathbf{k}'-\mathbf{k}}} + 2\nu_{\mathbf{k}'-\mathbf{k}}\omega'(-\omega_n)^{2\nu_{\mathbf{k}'-\mathbf{k}}-1} + O(\omega'^2)] \end{aligned}, \tag{58}$$

where a factor of $i^{2\nu_{k'-k}-1}$ was absorbed into the constant for notational convenience. Next we turn to the whole fraction containing the frequency dependence and expand it linearly, as

$$\begin{aligned} &G_{GR}(\mathbf{k},i\omega_n)G_{GR}(\mathbf{k}'-\mathbf{k},i(\omega'-\omega_n)) = \frac{1}{i(\omega'-\omega_n) - \varepsilon_{\mathbf{k}'-\mathbf{k}} + \mu - \Sigma(\mathbf{k}'-\mathbf{k},\omega'-\omega_n)} \\ &= \frac{1}{-i\omega_n - \varepsilon_{\mathbf{k}'-\mathbf{k}} + \mu - g_{\mathbf{k}'-\mathbf{k}}(-\omega_n)^{2\nu_{\mathbf{k}'-\mathbf{k}}}} - \frac{\omega'(1-2\nu_{\mathbf{k}'-\mathbf{k}}g_{\mathbf{k}'-\mathbf{k}}(-\omega_n)^{2\nu_{\mathbf{k}'-\mathbf{k}}-1})}{(-i\omega_n - \varepsilon_{k'-\mathbf{k}} + \mu - g_{\mathbf{k}'-\mathbf{k}}(-\omega_n)^{2\nu_{\mathbf{k}'-\mathbf{k}}})^2} + O(\omega'^2). \end{aligned} \tag{59}$$

Finally, taking the limit of $\omega' \to 0$ yields

$$G_{GR}(\mathbf{k}, i\omega)G_{GR}(-\mathbf{k}, -i\omega_n) = \frac{1}{i\omega_n - \varepsilon_{\mathbf{k}} + \mu - g_{\mathbf{k}}(\omega_n)^{2\nu_{\mathbf{k}}}} \frac{1}{-i\omega_n - \varepsilon_{\mathbf{k}'-\mathbf{k}} + \mu - g_{\mathbf{k}'-\mathbf{k}}(-\omega_n)^{2\nu_{\mathbf{k}'-\mathbf{k}}}}. \tag{60}$$

The Green's function can be directly connected to the spectral function, fact that will prove useful in this ladder diagram calculation since spectral functions are continuous in their domain. This relation is given in the previous section in Eq.(14). Applying the same logic to the second-order collective field expansion term $\Xi(T)$

$$\Xi(T) = -\frac{1}{\hbar^2\beta}\int \frac{d\mathbf{k}}{(2\pi)^2}\sum_n G_{GR}(\mathbf{k}, i\omega_n)G_{GR}(-\mathbf{k}, -i\omega_n). \tag{61}$$

Now we convert the sum into a contour integral in the same spirit as Eq.(35) along the contour C engulfing the upper complex plane. Before performing the integration we consider the additional term which corresponds to the Matsubara frequencies. The multiplication with the Matsubara term $lim_{\eta\to 0}\frac{\pm\hbar\beta e^{\eta z}}{e^{\hbar\beta z}\mp 1}$ only deforms the contour in a way that the Matsubara frequencies can be included in the calculation

$$\Xi(T) = -\frac{1}{2\pi i\hbar} lim_{\eta\to 0}\int \frac{d\mathbf{k}}{(2\pi)^2}\oint_C \int\int d\omega d\omega' d\omega'' \frac{\rho(\mathbf{k}, \omega')}{\omega' - i\omega}\frac{\rho(-\mathbf{k}, \omega'')}{\omega'' + i\omega}\frac{\pm\hbar\beta e^{\eta\omega}}{e^{\hbar\beta\omega}\mp 1}. \tag{62}$$

The ω integration has been transformed in this way so only two first-order poles appear, one being $\omega = -i\omega'$ and the second $\omega = i\omega''$. In order to solve the ω integral we enclose the contour in the upper complex plane so the first poles becomes valid for $Re[\omega'] < 0$ and the second one for $Re[\omega''] > 0$. Following this logic we are free to write the $\Xi(T)$ parameter as a sum of the heavy-side step functions $\theta(-\omega')$ and $\theta(\omega'')$ for the zero temperature limit [17] but since we have expanded into the whole complex plane these are replaced by the Fermi-Dirac distribution functions for the fermionic case

$$\Xi(T) = -\frac{1}{\hbar}\int \frac{d\mathbf{k}}{(2\pi)^2}\int\int d\omega' d\omega'' \rho(\mathbf{k}, \omega')\rho(-\mathbf{k}, \omega'')\frac{n_{FD}(\omega') - n_{FD}(-\omega'')}{\omega' + \omega''}. \tag{63}$$

3.5 Non-interacting case

Stripping the self-energy from our equations can provide a simplified relation, known from the BCS theory, which will later allow for a direct comparison with the interacting scheme. The spectral function in this non-interacting case obtains a couple

of handy properties. Firstly, it is symmetric in regards to momenta, meaning $\rho(\mathbf{k},\omega)=\rho(-\mathbf{k},\omega)$, and secondly, as shown beforehand, it can be transformed into a Dirac delta function

$$\Xi(T)=-\frac{1}{\hbar}\int\frac{d\mathbf{k}}{(2\pi)^2}\int\int d\omega' d\omega''\delta(\omega'-\frac{\varepsilon_{\mathbf{k}}-\mu}{\hbar})\delta(\omega''-\frac{\varepsilon_{\mathbf{k}}-\mu}{\hbar})\frac{n_{FD}(\omega')-n_{FD}(-\omega'')}{\omega'+\omega''}$$
$$=-\int\frac{d\mathbf{k}}{(2\pi)^2}\frac{n_{FD}(\frac{\varepsilon_{\mathbf{k}}-\mu}{\hbar})-n_{FD}(-\frac{\varepsilon_{\mathbf{k}}-\mu}{\hbar})}{2(\varepsilon_{\mathbf{k}}-\mu)}. \tag{64}$$

Following the identity $\frac{1}{1+e^{-2z}}-\frac{1}{1+e^{2z}}=\tanh(z)$ leads to further simplifications

$$\Xi(T)=\int\frac{d\mathbf{k}}{(2\pi)^2}\frac{\tanh(\beta(\varepsilon_{\mathbf{k}}-\mu)/2)}{2(\varepsilon_{\mathbf{k}}-\mu)}. \tag{65}$$

Additionally, we transform the momentum integration to an energy one by considering a two-dimensional distribution of momentum

$$\int\frac{d\mathbf{k}}{(2\pi)^2}=\frac{1}{(2\pi)^2}\int_0^{2\pi}d\phi\int_{-\infty}^{\infty}kdk=\frac{m}{\pi\hbar^2}\int_0^{\infty}d\varepsilon. \tag{66}$$

An additional factor of 2 was added in the above equation to include the spin degeneracy of fermions. Using the more convenient variables $x=\frac{\varepsilon_k}{\mu}$ and $y=\frac{\beta\mu}{2}$ transforms the ladder diagram by the equation into

$$\Xi(T)=\frac{m}{2\pi\hbar^2}\int_0^{\infty}dx\frac{\tanh(y(x-1))}{(x-1)}=\frac{m}{2\pi\hbar^2}\int_{-1}^{\Lambda}dx\frac{\tanh(yx)}{x}. \tag{67}$$

The substitution of the upper limit of the integral with a cut-off quantity Λ is necessary to mask this divergent integral. This problem is usually solved by the renormalization group, after the calculation of the observables, but in this context we will follow a more direct approach

$$\Xi(T)=\frac{m}{2\pi\hbar^2}\{\int_0^1 dx\frac{\tanh(yx)}{x}+\int_0^{\Lambda}dx\frac{\tanh(yx)}{x}\}=\frac{m}{2\pi\hbar^2}\{\int_0^1 dx\frac{\tanh(yx)}{x}+\int_0^{\Lambda}dx\frac{\tanh(yx)}{x}\}. \tag{68}$$

By partial integration the terms inside the integral become

$$\int_0^a dx\frac{\tanh(yx)}{x}=ln(a)tanh(ya)-\int_0^a\frac{yln(x)}{\cosh(yx)^2}$$
$$=ln(a)+\gamma-ln(\frac{\pi}{4y}),$$

where the symbol γ is used for the Euler-Mascheroni constant and the term $tanh(ya)$ is considered to be equal to one for $a >> 1$. Putting everything together yields

$$\Xi(T) = \frac{m}{2\pi\hbar^2}\{ln(\Lambda) + \gamma - ln(\frac{\pi}{2\beta\mu})\}. \tag{69}$$

The first term of the above equation holds all the divergences and as a result blows up our result to infinity. In order to avoid it in a delicate but not intrusive way, we can subtract from our result the background contribution that is inherit to the system. This can be easily found as it is equal to the zero temperature result of the ladder diagram. Applying the above rational to Eq.(65) we find the background contribution as

$$\begin{aligned}\Xi(0) &= lim_{y\to\infty}\frac{m}{2\pi\hbar^2}\{\int_0^1 dx\frac{\tanh(yx)}{x-1} + \int_0^\Lambda dx\frac{\tanh(yx)}{x-1}\} \\ &= lim_{y\to\infty}\frac{m}{2\pi\hbar^2}\{ln(\Lambda) - \int_0^1 dx\frac{yln(x)}{\cosh(yx)^2} - \int_0^\Lambda dx\frac{yln(z)}{\cosh(yx)^2}\}.\end{aligned} \tag{70}$$

The last two terms tend to zero for zero temperature leaving us with just one correction term exactly equal to the divergences found before. Considering the point of phase transition, the second-order coefficient in Eq.(52) is taken as positive [16] and the critical temperature can be found in regards to the systems parameters by taking $a(T_c) = 0$ for

$$T_c = \frac{2\mu}{\pi k_B}e^{\gamma - \frac{2\pi\hbar^2}{V_0 m}}. \tag{71}$$

Taking into consideration that the constant V_0 originates from the fourth order interaction means that it can be rewritten in regards to a dimensionless constant as $\frac{4\pi\hbar^2}{m}\lambda$. With this transformation the exponential quantity of the previous relation is written in its dimensionless form

$$T_c = \frac{2\mu}{\pi k_B}e^{\gamma - \frac{1}{2\lambda}}. \tag{72}$$

3.6 Expanding about the Fermi surface

Specifying the calculation of the previous subsection close to the Fermi surface we expand the spectral function's pole location linearly, so $\frac{\varepsilon_k - \mu}{\hbar} \approx v_B(\mathbf{k} - k_F)$. This transforms Eq.(63) into

$$\begin{aligned}\Xi(T) &= -\frac{1}{\hbar}\int\frac{d\mathbf{k}}{(2\pi)^2}\int d\omega' d\omega''\delta(\omega' - \hbar v_F(\mathbf{k}-k_F))\delta(\omega'' - \hbar v_F(\mathbf{k}-k_F))\frac{n_{FD}(\omega') - n_{FD}(-\omega'')}{\omega' + \omega''} \\ &= -\frac{1}{4\pi\hbar^2}\int_{-\infty}^{\infty} dk\, k\, \frac{n_{FD}(\hbar v_F(k-k_F)) - n_{FD}(-\hbar v_F(k-k_F)}{v_F(k-k_F)},\end{aligned} \tag{73}$$

where Eq.(67) was used to transform the momentum integral into its one-dimensional form. This produces four quantities inside the integral where the first two are just the Fermi-Dirac functions defined above. The result of the first two integrals can be found by substituting $k \to k - k_F$ as

$$-\frac{1}{4\pi\hbar^2 v_F}\int_{-\infty}^{\infty} dk n_{FD}(\hbar v_F k) - n_{FD}(-\hbar v_F k) = -\frac{1}{4\pi\hbar^2 v_F}(-ln(e^{\beta\hbar v_F k}+1) - ln(e^{-\beta\hbar v_F k}+1))\Big|_{-\Lambda}^{\Lambda}. \tag{74}$$

These two terms cancel each other out leaving us with two final terms to calculate, namely

$$-\frac{k_F}{4\pi\hbar^2}\int_{-\infty}^{\infty} dk \frac{n_{FD}(\hbar v_F(k-k_F)) - n_{FD}(-\hbar v_F(k-k_F))}{k-k_F} = \frac{k_F}{4\pi\hbar^2 v_F}\int_{-\infty}^{\infty} dk \frac{tanh(\beta\hbar v_F(k-k_F))}{k-k_F}. \tag{75}$$

The integration parameters can now change to $x = k/k_F - 1$ and $y = \frac{\beta\hbar v_F k_F}{2}$ so

$$\frac{k_F}{4\pi\hbar^2 v_F}\int_{-\infty}^{\infty} dx \frac{tanh(yx)}{x}. \tag{76}$$

Taking into consideration that the hyperbolic tangent is odd, the quantity inside the integral becomes even allowing for a change of integration boundaries. To get the desired result the only thing left to do is set the cutoff tending to a high value Λ, as

$$\Xi(T) = \frac{k_F}{2\pi\hbar^2 v_F}\int_0^{\Lambda} dx \frac{tanh(yx)}{x} = \frac{k_F}{2\pi\hbar^2 v_F}\{ln(\Lambda) + \gamma - ln(\frac{\pi}{2\beta\hbar v_F k_F}))\}. \tag{77}$$

The result of this integral has been done in Eq.(70) and proves that the critical temperature calculations lead to the same predictions when expanding linearly in regards to momentum. Moreover this allows for a direct implementation of the interaction corrections by defining the effective Fermi velocity given by the momentum dependence of the frequency pole in the spectral function. From that point a shortcut is created to calculate the critical temperature as

$$T_c = \frac{\hbar^2 k_F^2}{\pi k_B m^*} e^{\gamma - \frac{m}{2m^*\lambda}}. \tag{78}$$

Here the interacting Fermi velocity is taken as $\frac{\varepsilon_k - \mu - gRe[\Sigma(k,\omega)]}{\hbar} \approx v_F(\mathbf{k} - k_F)$ where m^* is the effective mass instead of $v_B = \frac{k_F}{m}$ which is the bare Fermi velocity.

3.7 Momentum-independent critical exponent at optimal doping

The spectral function, including interactions, is given in Eq.(14) and its contribution to the ladder diagram is shaped by the imaginary part of the self-energy. We claim that

this imaginary self-energy leads to a null result except for when a pole $\xi_{\mathbf{k}}$ is present. In the previous sections we have delved into this claim and realize the conditions where it holds true in more detail. The position of the pole is then given by

$$\xi_{\mathbf{k}} = \frac{\varepsilon_{\mathbf{k}} - \mu}{\hbar} + g\xi_{\mathbf{k}}^{2\nu_{\mathbf{k}}} cos((\nu_{\mathbf{k}} - \frac{1}{2})\pi). \tag{79}$$

Accordingly the spectral function is transformed into $\rho(\mathbf{k},\omega) = \delta(\omega - \xi_{\mathbf{k}})$. Following this approach allows easy implementation of the self-energy contribution into the critical temperature calculations by simply changing the location of the spectral function's pole. Directing our focus on the above equation the pole can be found, in regards to the system's parameters, by a recursive relation for $\xi_{\mathbf{k}}$ or numerical approximations. To extract this result we turn to the critical exponent $\nu_{\mathbf{k}} = \nu(1 - \frac{\mathbf{k}-k_F}{k_F})$, where most of our simplifications will take place. Since the self-energy formula is effective for momenta close to the Fermi surface, the most simplistic approximation would be to calculate the self-energy contribution given a momentum independent exponent $lim_{\mathbf{k}\to k_F}\nu_{\mathbf{k}} = \nu = \frac{1}{2}$. In the case of optimal doping this constant takes the value of half [5]. The pole is calculated to be

$$\xi_{\mathbf{k}} = \frac{\varepsilon_{\mathbf{k}} - \mu}{1 - g}. \tag{80}$$

It bares mention that in this framework the imaginary part of the self-energy, being $Im[\Sigma(\mathbf{k},\omega)] \propto lim_{\mathbf{k}\to k_F} sin((\nu_{\mathbf{k}} - \frac{1}{2})\pi) = 0$, fulfills the criteria for treating the spectral function as a delta function. This becomes more apparent if we rewrite the spectral function as a functional of the self-energy

$$\rho(\mathbf{k},\omega) = \frac{1}{\pi}\frac{-\mathrm{Im}(\Sigma(\mathbf{k},\omega)]}{(\omega - c_{\mathbf{k}} - \mathrm{Re}[\Sigma(\mathbf{k},\omega)])^2 + (\mathrm{Im}[\Sigma(\mathbf{k},\omega)])^2}. \tag{81}$$

Following the same procedure as Sec.(3.1) the ladder diagram contribution yields

$$\begin{aligned}\Xi(T) &= -\frac{1}{\hbar}\int \frac{d\mathbf{k}}{(2\pi)^2}\int\int d\omega' d\omega'' \delta(\omega' - \frac{c_{\mathbf{k}}}{1-g})\delta(\omega'' - \frac{c_{\mathbf{k}}}{1-g})\frac{n_{FD}(\omega') - n_{FD}(-\omega'')}{\omega' + \omega''} \\ &= -\int \frac{d\mathbf{k}}{(2\pi)^2}\frac{n_{FD}(\frac{c_{\mathbf{k}}}{1-g}) - n_{FD}(-\frac{c_{\mathbf{k}}}{1-g})}{2c_{\mathbf{k}}}.\end{aligned} \tag{82}$$

Manipulating the momentum integral into an energy integral we find that the resulting quantity differs slightly from that of Eq.(65) as in this case the $\Xi(T)$ quantity is given by

$$\Xi(T) = \frac{m(1-g)}{2\pi\hbar^2}\int_{-1}^{\Lambda} dx \frac{\tanh(yx)}{x}. \tag{83}$$

This time the integration variables equate to $x = \frac{\varepsilon_{\mathbf{k}}}{\mu}$ and $y = \frac{\beta\mu}{2(1-g)}$. Following the same integration process as the non-interacting case the renormalized contribution of the ladder diagram is calculated

$$\Xi(T) = \frac{m(1-g)}{2\pi\hbar^2}\{\gamma - ln(\frac{\pi(1-g)}{2\beta\mu})\}. \tag{84}$$

Leading to a critical temperature of

$$T_c^* = \frac{2\mu}{\pi k_B(1-g)} e^{\gamma - \frac{1}{2\lambda(1-g)}}, \tag{85}$$

where the fourth-order interaction constant has been rewritten in regards to the coupling constant λ in the same way as before. The implementation of the self-energy has apparent effects on the critical temperature equation, where the quantity of most importance is the fraction of the interactive critical temperature over the non interactive one. For this reason we define as $\sigma(g,\nu) = \frac{T_c^*}{T_c}$ the amplification factor

$$\sigma(g, 0.5) = \frac{e^{\frac{-g}{2\lambda(1-g)}}}{1-g}. \tag{86}$$

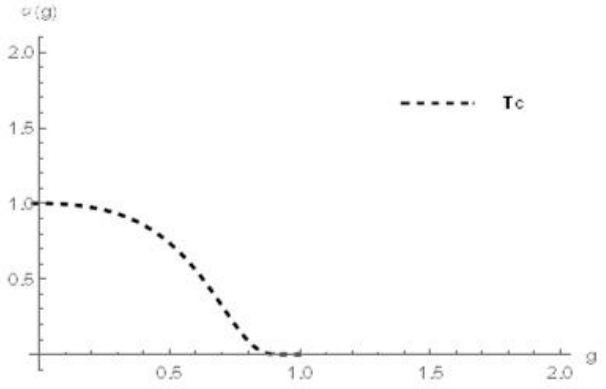

Figure 13: Multiplication factor for the critical temperature with momentum independent critical exponent at abstract doping.

The decreasing magnitude of Fig.(10) suggests that the maximal value can only be reached in the non-interactive case where the coupling constant is zero, meaning that the interaction attributes negatively to the critical temperature.

3.8 Linear momentum dependence for $\nu_k \geq \frac{1}{2}$

We now attempt to include into our calculations the momentum dependence of the critical exponent partially, by expanding in linear powers of **k**. In this section the

imaginary part of the self-energy will be considered negligible as discussed in Sec.(2.2). This simplification comes from the lack of mathematical machinery to derive the critical temperature with this additional term analytically. On the other hand it tests the ability of the Gubser-Rocha self-energy to predict a high critical temperature as the real part of the self-energy is the most contributing in this calculation and it does not share the experimental backing that the imaginary part has [5]. Considering the position of the pole given in Eq.(79), we Taylor expand close to the Fermi surface

$$\xi_{k_F}+(\mathbf{k}-k_F)\xi'_{k_F}=v_B\hbar(\mathbf{k}-k_F)+g(\xi_{k_F}^{2\nu}-2\xi_{k_F}^{2\nu-1}(\mathbf{k}-k_F)(\xi'_{k_F}-\frac{\xi_{k_F}ln(\xi_{k_F})}{k_F})). \tag{87}$$

This expansion leads to divergences given that $\xi_{\mathbf{k_f}}$ should tend to zero coming from the critical exponent terms. For this reason we apply the approximation derived on Sec.(2.2) to extract our result. The solutions for the frequency pole are given by

$$\xi_k=\frac{1-g(a+b(\nu_k-1)+c(\nu_k-1)^2)}{g(d+f(\nu_k-\frac{1}{2})+l(\nu_k-1/2)^2)}\pm\sqrt{\frac{1-g(a+b(\nu_k-1)+c(\nu_k-1)^2)}{g(d+f(\nu_k-\frac{1}{2})+l(\nu_k-1/2)^2)}^2+\frac{\varepsilon_k-\mu}{\hbar g(d+f(\nu_k-\frac{1}{2})+l(\nu_k-\frac{1}{2})^2)}}, \tag{88}$$

which when linearly expanding yields

$$\begin{aligned}
\xi'_{k_F}&=-R'_{k_F}\pm\frac{R_{k_F}R'_{k_F}+\frac{\hbar v_B}{2g(d+f(\nu-\frac{1}{2})+l(\nu-\frac{1}{2})^2)}}{R_{k_F}},\\
R_{k_F}&=\frac{1-g(a+b(\nu-1)+c(\nu-1)^2)}{2g(d+f(\nu-\frac{1}{2})+l(\nu-\frac{1}{2})^2)},\\
R'_{k_F}&=\frac{-\nu}{k_Fg}\{\frac{(f\nu-2l(\nu-\frac{1}{2})\nu)(1-g(a+b(\nu-1)+c(\nu-1)^2))+g\nu-2gc\nu(\nu-1)}{2(d+f(\nu-\frac{1}{2})+l(\nu-\frac{1}{2})^2)}\}.
\end{aligned} \tag{89}$$

One of the solutions shown above leads to an unphysical result. This comes from the quadratic approximation of the real part of the self-energy which can provide only one pole for the spectral function as mentioned before in Sec.(2). Considering only the physical solution, the effective mass is calculated to be

$$m^*=m[1-g(a+b(\nu-1)+c(\nu-1)^2)]. \tag{90}$$

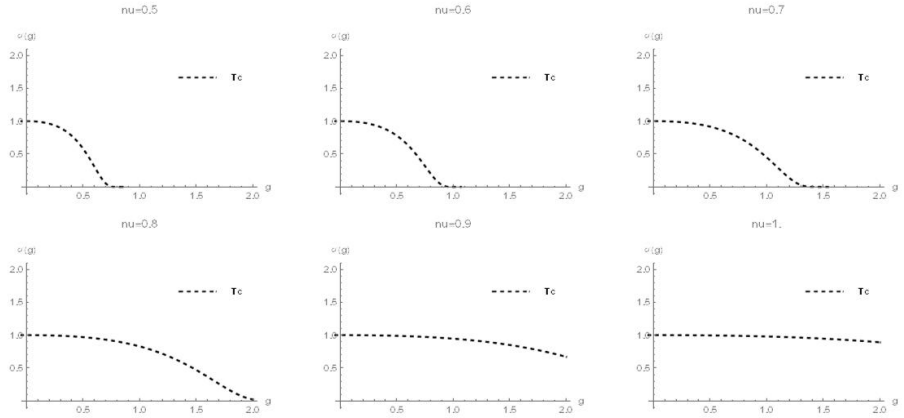

Figure 14: Critical temperature for varying values of doping.

The amplification factor can now be calculated as

$$\sigma(g,\nu)=\frac{e^{\frac{-g(a+b(\nu-1)+c(\nu-1)^2)}{2\lambda(1-g(a+b(\nu-1)+c(\nu-1)^2))}}}{1-g(a+b(\nu-1)+c(\nu-1)^2)}. \tag{91}$$

The maximal value is again found at the zero coupling constant range, while in the case of non-optimal doping this range grows as shown in Fig.(14).

Discussion

4.1 Analyticity and approximations

The matching of the Gubser-Rocha self-energy with the condensed-matter formalism was done with the latter as a priority. The intricacy of the momentum-dependent exponent is the self-energy of this theory was reduced by restricting the coupling constant to the experimental critical exponent range. This was done by fixing its sign to the predicted sign to battle the fact that the experimental terms are thought to be already renormalized by a renormalization procedure outside the scope of standard condensed matter physics. Given the fact that no information about the UV region of a theory can be extracted from the IR results fixing the sign was a one-way road. The analyticity of the Green's function was protected for the $\nu_k \leq \frac{1}{2}$ while for the $\nu_k \geq \frac{1}{2}$ case, which was of most interest, this was not true. The addition of the $c_k = \frac{\varepsilon_k - \mu}{\hbar}$ term creates poles in the upper and lower complex plane in positions that were problematic. The position of these points highly depend on the value of the critical exponent where increasing its value multiplies them, as shown in Fig.(15), with immediate

repercussions in regards to the spectral function normalizing to unity. This was circumvented by the approximation of Eq.(19) which is based on the Lagrange inversion theorem. It was found to approximately make the spectral function valid to the sum rule although the non-isolated singularities on the complex plane had to be neglected ad hoc. What is most surprising is that the position of this complex pole lies in the second Riemann sheet of the Green's function as shown in Fig.(11).

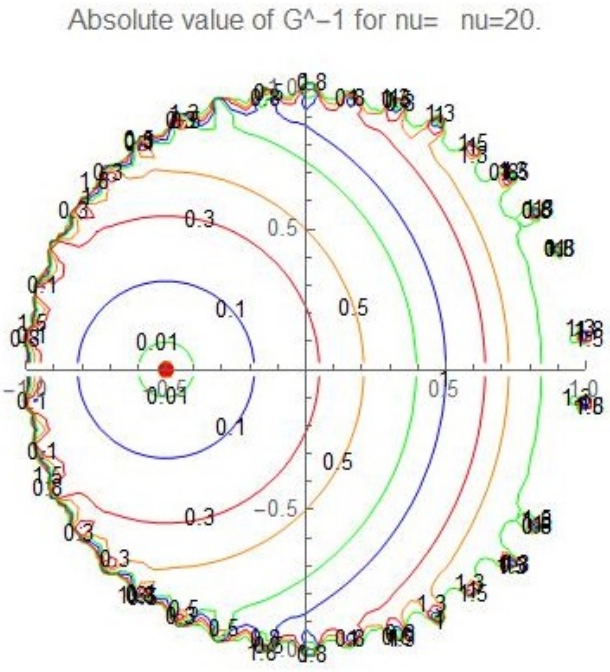

Figure 15: Inverse Green's function for a comparably big value of critical exponent.

This pole never reaches the physical sheet but affects its value on the real axis and more specifically the real part of the spectral function pole. Its potency is studied in Fig.(7) where a spectral function constructed with it showed agreement with the experimentally derived spectral function but only for a specific range of parameters.

The intricate behaviour of the power-law relation of the Gubser-Rocha self-energy was then simplified to a, up to quadratic order, numerical approximation, which also made the integrals of Sec.(3) solvable. As mentioned before, only one pole is valid from this approximation as the quadratic behaviour extends outside of the standard condensed matter physics and the experimental range. Additionally, the imaginary part of the spectral function was evaluated in Fig.(7) and a preferable range of critical exponent was found were the spectral function appeared to behave in a similar way as a Dirac delta function. The lack of mathematical tools to battle such imaginary term for the critical temperature calculation was the reason for this approximation as well as

putting the real part of the self-energy on the forefront. In this way the real part can be isolated and studied whether it contributes to the apparent high temperature behaviour of strange metals.

4.2 Critical Temperature

The second quantization background built in Sec.(3) is an attempt to conjugate the normal BCS prediction by correcting it with the self-energy added in Sec.(2). The linear expansion of the energy in regards to momentum was done with the purpose of simplifying the calculation procedure that leads to critical temperature estimations. The whole theoretical formalism was built for a two-dimensional system in order to replicate the experiment's conditions where a single layer of $(Pb,Bi)_2Sr_{2-x}La_xCu_{6+\delta}$ was isolated. After the inclusion of the interaction terms the resulting critical temperature was put against the non-interacting one as a function of the coupling constant, shown in Fig.(13) and Fig.(14). As mentioned before this restriction goes hand in hand with the critical exponent range that we study. In the case of doping dependent critical temperature the fitting equation for the spectral function's pole was employed in order to find the effective mass of the system. At first glance the result seems irrelevant to the quadratic momentum dependence of the real self-energy, as the three fitting parameters (d,f,l) are absent in the effective mass equation, although its contribution is present in the (a,b,c) parameters too. One can easily see that the result of Eq.(91) differs than that described in Eq.(86) for the case of optimal doping since the numerical approximation estimates a uniform solution for the whole range of the critical exponent. This means that both the linear and quadratic frequency dependence inherently contribute to the result even at the extremums of the critical exponent range. Looking at Fig.(14) the doping parameter acts as a smoothening factor for the contribution of the real self energy as more values of the coupling constant maintain a higher T_c.

Although the real part can provide intuition in regards to the behaviour of the interacting system the imaginary self-energy is a point of great interest as well, especially when one considers its increasing contribution while approaching the phase transition point, shown in Fig.(8). The approximatory approach built throughout the script is deficient in taking that into account, making it a potential candidate for the high temperature superconductive behaviour of the strange metal.

Conclusion

The efforts of scientists continue as high temperature superconductivity remains an open problem for more that 30 years. The strong electron glue that forces the cuprate metal to condense avoids any standard theoretical approach while identifying the microscopic quantities required for a quantum description is a highly demanding process. The Gubser-Rocha form of self-energy, being the only verified elucidation of the ARPES data, is shown to have intricate properties when coming to the standard condensed-matter theory. Its unique analytically continued image requires special handling in order for it to fit the known formalism. Given approximatory and numerical procedures this script mends part of the divergences.

The formalism for including the Gubser-Rocha real self-energy was built where the critical temperature equations for the strange metal at optimal doping and at abstract doping were derived. Concerning the high-temperature superconductive behaviour no indication of an increase in critical temperature was found leaving a lot to be expected from the inclusion of the imaginary part of the same self-energy, which is left for future research. Additionally, further analysis on the coupling constant can provide a more direct connection with the experimental evidence since its relation to the fitting parameter λ, shown in Eq.(11), is readily available. With this matching the exact contribution of the real part of the self-energy can be found for $(Pb,Bi)_2Sr_{2-x}La_xCu_{6+\delta}$ metals specifically.

Having critical temperature far above the predicted value, strange metals have gained a great amount of scientific interest. Understanding the physics that dictates the thermodynamic behaviour of this class of metals allows for a plethora of technological applications. Although the theoretical-physics tool box has evolved in new striking theories in order to find common grounds with the experimental perspective, the elusive nature of the cuprate's microscopic interactions appear just only out of reach.

Bibliography

[1] O'Mahony, S. M., et al. "On the electron pairing mechanism of copper-oxide high temperature superconductivity."
url arXiv preprint arXiv:2108.03655 (2021)

[2] Maldacena, Juan. "The large-N limit of superconformal field theories and supergravity." International journal of theoretical physics 38.4 (1999): 1113-1133.

[3] Hartnoll, Sean A., Andrew Lucas, and Subir Sachdev. Holographic quantum matter. MIT press, 2018

[4] Gubser, Steven S., and Jie Ren. "Analytic fermionic Green's functions from holography." Physical Review D 86.4 (2012): 046004.

[5] Smit, S., et al. "Momentum-dependent scaling exponents of nodal self-energies measured in strange metal cuprates and modelled using semi-holography." arXiv preprint arXiv:2112.06576 (2021).

[6] Valla, T., et al. "Evidence for quantum critical behavior in the optimally doped cuprate Bi2Sr2CaCu2O8+ ." Science 285.5436 (1999): 2110-2113.

[7] Negele, John W., and Henri Orland. Quantum many-particle systems. CRC Press, 2018.

[8] Gauntlett, Jerome P., Julian Sonner, and Daniel Waldram. "Universal fermionic spectral functions from string theory." Physical Review Letters 107.24 (2011): 241601.

[9] Beji, Serdar. "Polynomial Functions Composed of Terms with Non-Integer Powers." Advances in Pure Mathematics 11.10 (2021): 791-806.

[10] Faulkner, Thomas, et al. "Emergent quantum criticality, Fermi surfaces, and AdS 2." Physical Review D 83.12 (2011): 125002.

[11] Galindo, Alberto, and Pedro Pascual. Quantum mechanics II. Springer Science Business Media, 2012.

[12] Brown, Lowell S. Quantum field theory. Cambridge University Press, 1994

[13] Wolkanowski, Thomas. "Resonances and poles in the second Riemann sheet." arXiv preprint arXiv:1303.4657 (2013).

[14] Döring, M., et al. "Analytic properties of the scattering amplitude and resonances parameters in a meson exchange model." Nuclear Physics A 829.3-4 (2009): 170-209

[15] Blankenbecler, R., et al. "Singularities of scattering amplitudes on unphysical sheets and their interpretation." Physical Review 123.2 (1961): 692.

[16] Stoof, Henk TC, Koos B. Gubbels, and Dennis Dickerscheid. Ultracold quantum fields. Springer, 2009.

[17] Nayak, Chetan. "Quantum Condensed Matter Physics." Lecture Notes (2004): 1-17.